Polyhedron 158 (2019) 208–214

Contents lists available at ScienceDirect

Polyhedron

journal homepage: www.elsevier.com/locate/poly

Synthesis of a rhodium(III) triphenylphosphine complex via C—S bond cleavage of an azo-thioether ligand: X-ray structure, electrochemistry and catalysis towards transfer hydrogenation of ketones

Puspendu Roy [a,b], Chandan Kumar Manna [a], Rahul Naskar [a], Tapan Kumar Mondal [a,*]

[a] Department of Chemistry, Jadavpur University, Kolkata 700032, India
[b] Department of Chemistry, Netaji Nagar Day College, University of Calcutta, Kolkata 700092, India

ARTICLE INFO

Article history:
Received 12 July 2018
Accepted 13 October 2018
Available online 1 November 2018

Keywords:
Rhodium(III) complex
C—S bond cleavage
Electrochemistry
Transfer hydrogenation
DFT calculation

ABSTRACT

A new rhodium(III) triphenylphosphine complex having the general formula $[Rh(PPh_3)_2(L)Cl]$ (**1**) was synthesized by C—S bond cleavage of an ONS donor azo-thioether ligand (L-CH_2Ph). The complex was thoroughly characterized by various spectroscopic techniques. Its single crystal X-ray structure exhibits an octahedral geometry around the rhodium(III) center. A cyclic voltammogram of the complex exhibits ligand based quasi-irreversible oxidative and reductive responses. The electronic structure, redox properties and electronic excitations in the complex were interpreted by DFT and TDDFT calculations. The complex effectively catalyzed the transfer hydrogenation reaction of ketones with high yields in *i*-PrOH in the presence of a base.

1. Introduction

There has been growing interest in transition metal mediated activation of carbon–sulfur bonds due to its importance in the fuel and coal industry for decades [1–4]. Transition metal mediated C—S bond activation and cleavage also play a vital role in the field of bioorganic and synthetic chemistry [5,6]. In order to improve the desired reactivities of metal catalyzed C—S bond activation, the design of ligand systems are important. By the adjustment of the binding affinity and the size of the ligand, both the electron density and steric factors at the metal center can be tuned in the complexes. The phosphine group PR_3 (R = alkyl, aryl, alkoxy etc.) is one of the important ligands used in organometallic chemistry for C—H and C—S activations. The effects on M—L bonds with the variation of the electronic and steric natures of the R group of PR_3 ligands are well quantified by Tolman [7,8]. Moreover, transition metal mediated C—S bond activation along with the transformation processes are of stimulating interest from the perspective of synthetic, mechanistic as well as catalytic aspects [9–12].

In recent years, catalytic transfer hydrogenation has received considerable attention because of its capacity to hydrogenate substrates under mild conditions and it avoids the use of high pressure vessels and compressed H_2 or moisture-sensitive hydride reagents [13,14]. Continuous research is going on to develop new technologies for future industrial applications in terms of selectivity, efficiency, scope, simplicity and economic viability [15,16]. So, the development of new catalysts for the transfer hydrogenation of ketones is still of considerable interest. Currently, we are working on the design and development of ruthenium, rhodium and osmium metal complexes as catalysts in the transfer hydrogenation of ketones [17–19]. In the present contribution, we have synthesized a new rhodium(III) triphenylphospine complex, $[Rh(PPh_3)_2(L)Cl]$ (**1**), via C—S bond cleavage of a thioether containing ligand, 3-(2-(2-((pyridin-2-ylmethyl)thio)phenyl)hydrazono)pentane-2,4-dione (L-CH_3). The complex effectively catalyzes the transfer hydrogenation reaction of ketones in *i*-PrOH. The structure of the complex was confirmed by the single crystal X-ray diffraction method. The electronic structure and redox properties of the complex are interpreted by DFT calculations.

2. Experimental

2.1. Material and methods

All the reagents and solvents were purchased from commercial sources and used as received. Acetylacetone and the inorganic metal salts were obtained from E. Merck, India. 2-Aminothiophe-

* Corresponding author.
E-mail address: tapank.mondal@jadavpuruniversity.in (T.K. Mondal).

https://doi.org/10.1016/j.poly.2018.10.061
0277-5387/

nol, 2-(chloromethyl)pyridine hydrochloride and $[Rh(PPh_3)_3Cl]$ were purchased from Sigma Aldrich. The ligand L-CH_2Ph was prepared by following the published procedure [20].

Microanalyses (C, H, N) data were obtained using a PerkinElmer Series-II CHN-2400 CHNS/O elemental analyzer. Electronic spectra were measured on a Lambda 750 PerkinElmer spectrophotometer in acetonitrile. IR spectra were recorded on a RX-1 PerkinElmer spectrometer in the range 4000–400 cm^{-1} with the samples in the form of KBr pellets. The NMR spectrum was recorded in $CDCl_3$ on a Bruker (AC) 300 MHz FT-NMR spectrometer in the presence of TMS as an internal standard. HRMS mass spectra were obtained on a Waters (Xevo G2 Q-TOF) mass spectrometer. Cyclic voltammetric measurements were carried out using a CHI electrochemical workstation. A platinum wire working electrode, a platinum wire auxiliary electrode and Ag/AgCl reference electrode filled with saturated KCl solution were used in a standard three-electrode configuration. The supporting electrolyte was 0.1 M tetrabutylammonium hexafluorophosphate, $[Bu_4N]PF_6$, and the solute concentration was *ca* 10^{-3} M. Before measurement, the solutions were degassed by bubbling N_2 through them for 5 min. The half-wave potential $E_{1/2}$ was set equal to $1/2(E_{pa} + E_{pc})$, where E_{pa} and E_{pc} are anodic and cathodic cyclic voltammetric peak potentials, respectively.

2.2. Synthesis of $[Rh(PPh_3)_2(L)Cl]$ (**1**)

0.190 g (0.2 mmol) $Rh(PPh_3)_3Cl$ was dissolved in 20 mL of acetonitrile. To this solution 0.065 g (0.2 mmol) L-CH_2Ph in 10 mL of acetonitrile was added. The reaction mixture was refluxed for 10 h under a N_2 atmosphere. The solvent was then removed under reduced pressure in a rotary evaporator. The crude product was dissolved in dichloromethane and purified by column chromatography using silica gel (mesh 60–120). A deep red coloured complex (**1**) was eluted by a 50% (v/v) ethyl acetate-petroleum ether mixture. On removal of the solvent under reduced pressure, the pure complex **1** was obtained as a red solid which was further dried under vacuum. Yield: 0.114 g, 64%.

Anal. Calc. for $C_{47}H_{40}ClN_2O_2P_2RhS$ (**1**): C, 62.91; H, 4.51; N, 3.11. Found: C, 62.92; H, 4.49; N, 3.12%; IR data (KBr, cm^{-1}): 1654 ν(C═O), 1355 ν(N═N). ^1H NMR data ($CDCl_3$, δ, ppm): 2.53 (3H, s), 2.67 (3H, s), 7.22–7.93 (34H, m). UV–Vis (in acetonitrile), λ_{max} (nm) ($\varepsilon \times 10^{-3}$, mol^{-1} cm^{-1}): 530 (6.13), 425 (sh.), 344 (11.44), 281 (25.38). HRMS *m*/*z*, 920.3256 $[M]^+$. Electrochemistry (in acetonitrile) (scan rate: 100 mV s^{-1}): $E_{1/2}$ = 1.06 V (ΔE = 116 mV) and E_{pc} = −1.12 V (ΔE, 140 mV).

2.3. Crystallography

Single crystals of **1** were obtained by slow diffusion of n-hexane into a dichloromethane solution of the complex. Single crystal data collection was performed with an automated Bruker SMART APEX CCD diffractometer using graphite monochromatized Mo Kα radiation (λ = 0.71073 Å). Reflection data were recorded using the ω scan technique. Unit cell parameters were determined from least-squares refinement of the setting angles with θ in the range $1.71 \le \theta \le 27.54°$. Out of 66 540 collected data, 9423 with $I > 2\sigma(I)$ within the $-30 \le h \le 31$, $-12 \le k \le 12$, $-46 \le l \le 46$ were used for the structure solution. The structure was solved and refined by full-matrix least-squares techniques on F^2 using SHELXL-2016/6 [21,46,47]. The absorption corrections were done by multi-scan (SHELXTL program package) and all the data were corrected for the Lorentz, polarization effect. Hydrogen atoms were included in the refinement process as per the riding model. Details of the crystal analysis, data collection and structure refinement data for **1** are given in Table 1.

Table 1
Crystallographic data for $[Rh(PPh_3)_2(L)Cl]$ (**1**).

Empirical formula	$C_{47}H_{40}ClN_2O_2P_2RhS$
Formula weight	897.17
Crystal system	monoclinic
Space group	*C*2/*c*
a (Å)	24.2017(6)
b (Å)	9.5376(3)
c (Å)	35.9841(10)
β (°)	100.072(2)
V (Å^3)	8178.1(4)
Z	8
ρ_{calcd} (g cm^{-3})	1.457
μ (m m^{-1})	0.654
T (K)	293(2)
hkl range	−30 to 31, −12 to 12, −46 to 46
F(0 0 0)	3680
θ range (°)	1.709–27.539
Reflections collected	66 260
Unique reflections (R_{int})	9391
Observed data ($I > 2\sigma(I)$)	7797
Data/restraints/parameters	9391/0/505
R_1[a], wR_2[b] ($I > 2\sigma(I)$)	0.0389, 0.0832
R_1, wR_2 (all data)	0.0498, 0.0891
Goodness-of-fit (GOF)[c]	0.977
Largest difference in peak/hole (e Å^{-3})	0.433 and −594

[a] $R_1 = \sum(|F_o| - |F_c|)/\sum|F_o|$.
[b] $wR_2 = \{\sum[w(F_o^2 - F_c^2)^2]/\sum[w(F_o^2)^2]\}^{1/2}$, $w = 1/[\sigma^2(F_o^2) + (0.0312P)^2 + 25.0278P]$, where $P = (F_o^2 + 2F_c^2)/3$.
[c] $GOF = \{\sum[w(F_o^2 - F_c^2)^2]/(n - p)\}^{1/2}$, where n = number of measured data and p = number of parameters.

2.4. Computational method

Geometry optimizations of $[Rh(PPh_3)_2(L)Cl]$ (**1**) and the oxidized species $\mathbf{1}^+$ were carried out by the DFT/B3LYP and DFT/UB3LYP methods, respectively [22,23]. All elements, except rhodium, were assigned the 6–31G(d) basis set. The LanL2DZ basis set with an effective core potential was employed for the rhodium atom [24–26]. A vibrational frequency calculation was performed to ensure that the optimized geometry represents the local minima and there are only positive eigenvalues. Vertical electronic excitations were computed using the time-dependent density functional theory (TDDFT) formalism [27–29] for **1** in acetonitrile using a conductor-like polarizable continuum model (CPCM) [30–32]. All computations were carried out using the GAUSSIAN09 (G09) program [33]. GaussSum [34] software was used to calculate the fractional contributions of various groups to each molecular orbital.

2.5. General procedure for the transfer hydrogenation of ketones

Typical procedure for the catalytic transfer hydrogenation reaction: A solution of the rhodium(III) complex (**1**) (0.0075 mmol), KOH (0.03 mmol) and the corresponding ketone (3 mmol) in 10 mL degassed *i*-PrOH was refluxed at 80 °C under stirring conditions. The reaction was monitored at various time intervals by GC. After the reaction was complete, 2-propanol was removed under reduced pressure on a rotary evaporator and the resulting semi-solid was extracted with diethyl ether (5 × 10 mL). To separate the catalyst, the ether extract was then passed through a short silica gel column and condensed under reduced pressure; conversion was determined by GC equipped with a flame ionization detector (FID) and an HP-5 column of 30 m length, 0.53 mm diameter and 5.00 μm film thickness. The column, injector and detector temperatures were 200, 250 and 250 °C, respectively. The carrier gas was N_2 (UHP grade) at a flow rate of 30 mL/min. The injection volume of the sample was 2 μL. The alcohols were identified by GC using undecane

as an internal standard and each of the catalytic runs was performed three times.

3. Results and discussion

3.1. Synthesis and spectral characterization

The octahedral rhodium(III) triphenylphosphine complex, [Rh(PPh_3)$_2$(L)Cl] (**1**) was synthesized by the reaction of Rh(PPh_3)$_3$Cl and the azo-thioether ligand L-CH_2Ph under refluxing conditions in acetonitrile (Scheme 1). The complex was thoroughly characterized by several spectroscopic techniques. The IR spectrum of the complex exhibits a sharp signal at 1654 cm^{-1}, which corresponds to ν(C=O), along with a weak peak at 1355 cm^{-1}, corresponding to ν(N=N). The ν(N=N) band is significantly shifted to a lower frequency region compare to the free ligand value, suggesting the coordination of azo-N atom to the rhodium ion [20]. The ^{1}H NMR spectrum of the complex was taken in $CDCl_3$. All the expected signals of the ligands, including aromatic protons, were resolved, except the S-CH_2Ph peaks, suggesting C—S bond cleavage in the complex. A series of overlapping multiplet signals appeared in the region δ 7.2–7.9 ppm, which correspond to the protons of the coordinated triphenylphosphine ligand in the complex. The UV–Vis spectrum of the complex in acetonitrile exhibits a low energy broad peak at 530 nm ($\varepsilon \times 10^{-3}$, 6.13 M^{-1} cm^{-1}) along with a shoulder at 425 nm. In addition, two ligand centered peaks appeared at 344 nm ($\varepsilon \times 10^{-3}$, 11.44 M^{-1} cm^{-1}) and 281 nm ($\varepsilon \times 10^{-3}$, 25.38 M^{-1} cm^{-1}) in acetonitrile (Fig. 1).

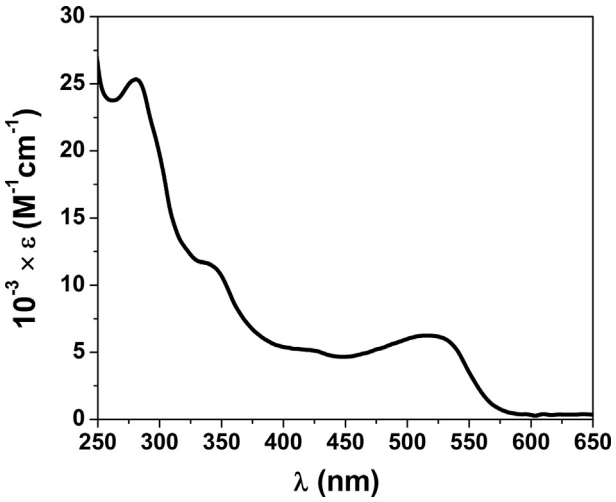

Fig. 1. UV–Vis spectrum of complex [Rh(PPh_3)$_2$(L)Cl] (**1**) in acetonitrile.

3.2. Molecular structure

The molecular structure of the complex [Rh(PPh_3)$_2$(L)Cl] (**1**) was confirmed by the single crystal X-ray diffraction method. Single crystals suitable for structure determination were grown by slow diffusion of n-hexane into a dichloromethane solution of the complex. The molecule crystallized in the monoclinic crystal system with *C*2/*c* symmetry. Selected bond lengths and bond angles are given in Table 2. An ORTEP plot with the atomic numbering scheme is shown in Fig. 2. The molecule consists of a central rhodium atom surrounded by six donor centers and it adopts a distorted octahedral geometry. The atomic arrangement involves two *trans*-PPh_3 ligands, chelating O,N,S donors and a Cl atom *trans* to the azo-N atom within the RhP_2ONSCl coordination sphere. The O,N,S donor thioether ligand binds through the O, azo-N and thiophenolato-S (formed by C—S bond cleavage) atoms to the rhodium centre in the complex. The rhodium coordination sphere deviates from an ideal octahedron because of the deviation of the chelate bite angle of the five membered ring (Rh1–N1–C6–C1–S1) [86.50 (6)°] from 90°. The Rh–P (Rh1–P1, 2.4109(7) and Rh1–P2, 2.3978

Table 2
X-ray and DFT calculated selected bond distances (Å) and angles (°).

Bonds (Å)	X-ray	Calc.	
		1	**1$^+$**
Rh1–N1	1.996(2)	2.035	2.038
Rh1–O1	2.0659(18)	2.095	2.103
Rh1–S1	2.3021(7)	2.347	2.308
Rh1–Cl1	2.3676(7)	2.437	2.422
Rh1–P1	2.4109(7)	2.481	2.504
Rh1–P2	2.3978(7)	2.442	2.522
N1–N2	1.266(3)	1.272	1.292
O1–C10	1.257(3)	1.269	1.256
S1–C1	1.746(3)	1.756	1.725
Bond angles (°)			
N1–Rh1–O1	90.23(8)	89.022	88.476
N1–Rh1–S1	86.50(6)	85.912	85.408
N1–Rh1–P1	89.78(6)	92.459	93.962
N1–Rh1–P2	91.21(6)	92.251	93.248
N1–Rh1–Cl1	179.78(8)	178.910	179.156
O1–Rh1–S1	176.72(5)	174.855	173.883
O1–Rh1–P1	89.72(5)	90.277	89.066
O1–Rh1–P2	89.11(5)	89.039	87.344
O1–Rh1–Cl1	89.96(5)	90.204	92.301
S1–Rh1–P1	90.44(3)	89.043	91.143
S1–Rh1–P2	90.79(3)	90.054	93.203
S1–Rh1–Cl1	93.31(3)	94.873	93.812
P1–Rh1–P2	178.47(2)	175.227	171.855
P1–Rh1–Cl1	90.12(2)	88.302	86.440
P2–Rh1–Cl1	88.89(2)	86.977	86.401
C1–S1–Rh1	97.19(9)	96.906	98.357

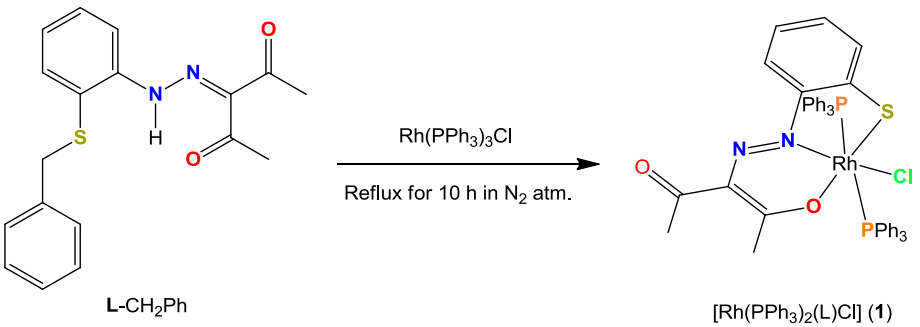

Scheme 1. Synthesis of the rhodium(III) complex, [Rh(PPh_3)$_2$(L)Cl] (**1**).

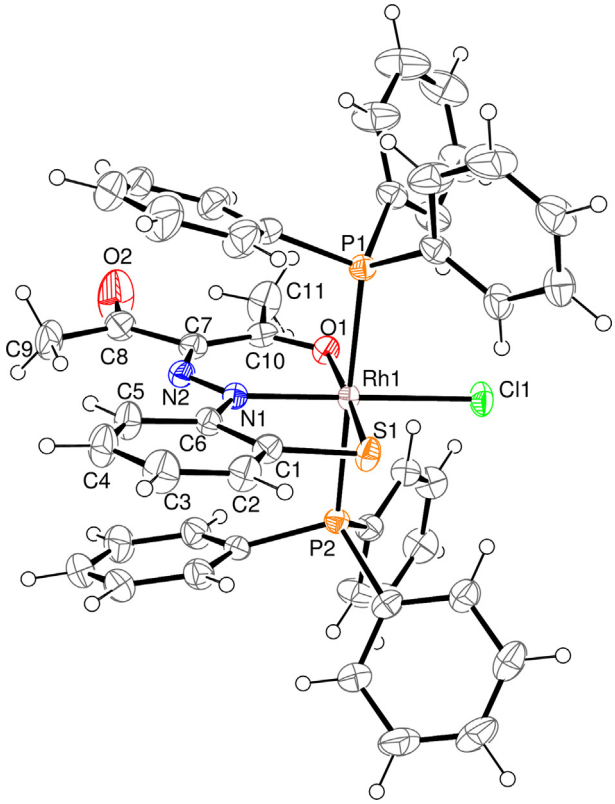

Fig. 2. ORTEP plot of **1** with 35% ellipsoidal probability.

(7) Å), Rh–Cl (Rh1–Cl1, 2.3676(7) Å) and Rh–S (Rh1–S1, 2.3021 (7) Å) bond distances are found to be as expected by comparison to similar rhodium triphenylphosphine complexes [18,35,36].

3.3. DFT and TDDFT calculations

To interpret the electronic structure of the complex, the geometry of **1** was optimized by the DFT/B3LYP method. DFT optimized bond distances and angles are well correlated with the X-ray crystal structure data (Table 2). The energy and compositions of selected molecular orbitals of **1** are summarized in Table 3. The HOMO of the complex has 88% ligand character and is mostly concentrated on the S atom. HOMO−1 has 79% π(L) character along

Table 3
Energy and composition of selected molecular orbitals of $[Rh(PPh_3)_2(L)Cl]$ (**1**).

MO	Energy (eV)	% of composition			
		Rh	L	PPh_3	Cl
LUMO+5	−0.65	0	01	98	0
LUMO+4	−0.65	02	09	88	0
LUMO+3	−0.71	01	0	99	0
LUMO+2	−1.19	50	37	04	9
LUMO+1	−1.76	30	24	44	02
LUMO	−1.88	09	80	11	0
HOMO	−4.84	04	88	08	0
HOMO−1	−5.64	15	79	03	03
HOMO−2	−5.97	25	39	05	30
HOMO−3	−6.06	09	08	40	43
HOMO−4	−6.22	08	70	04	18
HOMO−5	−6.45	10	14	66	10
HOMO−6	−6.64	0	04	95	0
HOMO−7	−6.7	02	07	90	01
HOMO−8	−6.75	06	34	47	14
HOMO−9	−6.78	01	11	88	0
HOMO−10	−6.82	02	13	82	04

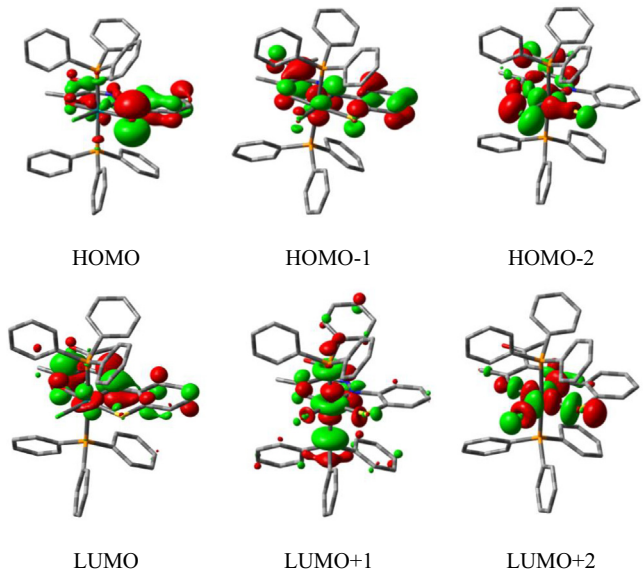

Fig. 3. Contour plots of selected molecular orbitals of **1**. Isodensity value 0.04 e $Bohr^{-3}$.

with a reduced contribution of *dπ*(Rh) (15%). HOMO−2 has mixed contributions of π(L), *dπ*(Rh) and *pπ*(Cl) orbitals. The LUMO of the complex has 80% π*(L) character, while LUMO1 and LUMO+2 have mixed contributions of *dπ*(Rh) (30–50%), π*(L) (24–37%) and π*(PPh_3) orbitals (Fig. 3).

The UV–Vis spectrum of the complex was interpreted using calculated vertical electronic transitions by the TDDFT method using the CPCM model in acetonitrile. The calculated vertical electronic transitions are summarized in Table 4. The experimental broad band at 530 nm corresponds to the admixture of HOMO → LUMO and HOMO → LUMO+1 transitions, having mixed ILCT (intra-ligand charge transfer transition) and LMCT (ligand to metal charge transfer transition) character. The low energy bands at 344 and 281 nm correspond to π(L) → π*(L) transitions, having ILCT character.

3.4. Electrochemistry

The electrochemical behavior of complex **1** was investigated by a cyclic voltammetric study in acetonitrile using tetrabutylammonium hexafluorophosphate $[Bu_4N]PF_6$ (0.1 M) as the supporting electrolyte and a Ag/AgCl reference electrode. The complex exhibits one quasi-reversible reduction couple with $E_{1/2}$ = −1.12 V (Δ*E* = 140 mV) along with a quasi-reversible oxidation couple with $E_{1/2}$ = 1.06 V (Δ*E* = 116 mV) (Fig. 4) within the experimental potential range of ±2.0 V *versus* the Ag/AgCl reference electrode in CH_3-CN. The peak at −1.12 V corresponds to the reduction of the azo (N=N) bond of the ligand as the LUMO of the complex has 80% π*(L) character with a major contribution of the azo(N=N) function. The quasi-reversible oxidation of **1** is likely to be associated with the Rh(III) to Rh(IV) oxidation [36] or oxidation of the thiophenolato-S to a thiyl radical [37–39]. The HOMO of complex **1** has 88% ligand character with a major contribution of the *pπ*(S) orbital (51%). So, the oxidation process is better assigned as the formation of the thiyl radical (S·) in comparison to the alternate possibility of Rh(III) to Rh(IV) oxidation. This was also further evidenced from DFT calculations of the oxidized species ($\mathbf{1}^+$) by the UB3LYP method. The *β*-spin LUMO of $\mathbf{1}^+$ has 91% ligand character with a major contribution from the *pπ*(S) orbital (53%) (Fig. 5). A spin density plot of $\mathbf{1}^+$ is majorly concentrated on the S atom and has only 1% contribution from the Rh atom, suggesting the oxida-

Table 4
Vertical electronic excitations calculated by the TDDFT/CPCM method for **1**.

$E_{excitation}$ (eV)	$\lambda_{excitation}$ (nm)	Osc. strength (f)	Key transitions	Character[a]	$\lambda_{expt.}$ (nm) ($\varepsilon \times 10^{-3}$, M^{-1} cm^{-1})
2.2471	551.8	0.0242	(67%) HOMO → LUMO+1 (28%) HOMO → LUMO	π(L) → π*(L)/dπ(Rh) (ILCT/LMCT)	530 (6.13)
2.4725	501.4	0.0888	(72%) HOMO → LUMO (26%) HOMO → LUMO+1	π(L) → π*(L)/dπ(Rh) (ILCT/LMCT)	
2.8431	436.1	0.0145	(69%) HOMO−1 → LUMO+1	π(L) → π*(L)/dπ(Rh) (ILCT/LMCT)	425 (sh.)
3.1573	392.7	0.0545	(62%) HOMO−1 → LUMO	π(L) → π*(L) (ILCT)	
3.4871	355.6	0.1307	(63%)HOMO−4 → LUMO	π(L) → π*(L) (ILCT)	344 (11.44)

[a] LMCT: Ligand to metal charge transfer transition and ILCT: Intra ligand charge transfer transition.

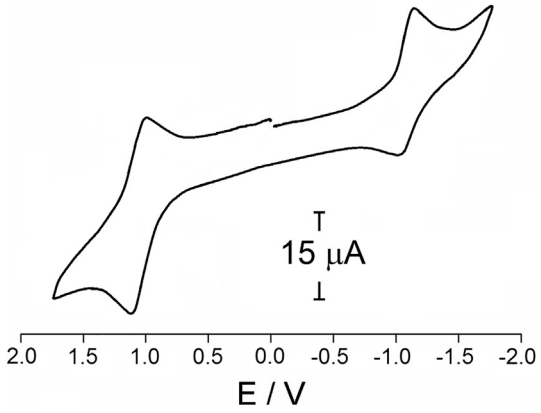

Fig. 4. Cyclic voltammogram of **1** in acetonitrile (Supporting electrolyte: 0.1 M tetrabutylammonium hexafluorophosphate, $[Bu_4N]PF_6$; solute concentration: $\sim 10^{-3}$ M; scan rate: 100 mV s^{-1}).

tion takes place on the thiophenolato-S atom to form the thiyl radical (S•) (see Fig. 6).

3.5. Catalytic transfer hydrogenation reactions

The transfer hydrogenation reaction is a significant and useful process in organic synthesis. The platinum group metal complexes have been used extensively as effective catalysts for transfer hydrogenation reactions [19,40–48]. In the present work, the catalytic properties of the synthesized rhodium(III) complex **1** towards transfer hydrogenation reactions of ketones were tested in *i*-PrOH in the presence of a base.

Complex **1** catalyzed the transfer hydrogenation of ketones at 80 °C with *i*-PrOH as the hydrogen source in the presence of a base. To evaluate the catalytic efficiency of the complex, the reaction conditions were optimized with variation of the base, reaction time and catalyst:substrate (C:S) ratios. The transfer hydrogenation of acetophenone to 1-phenylethanol was chosen as a standard reaction in *i*-PrOH and the results are summarized in Table 5. With a catalyst:substrate (C:S) ratio of 1:300, the conversion rates were significantly varied (39–98%) with the base employed. In the case of weak bases, such as Na_2CO_3 and CH_3COONa, the conversions were significantly low, whereas a moderate conversion was observed in the case of KO^{t}Bu. Significant catalytic conversions were achieved for strong bases such as KOH or NaOH. The progress of the reaction was also monitored over different time intervals and it was found that the formation of 1-phenylethanol initially increased and after 5 h there was no appreciable change in the conversion rate. Again, to understand the catalytic efficiency of the

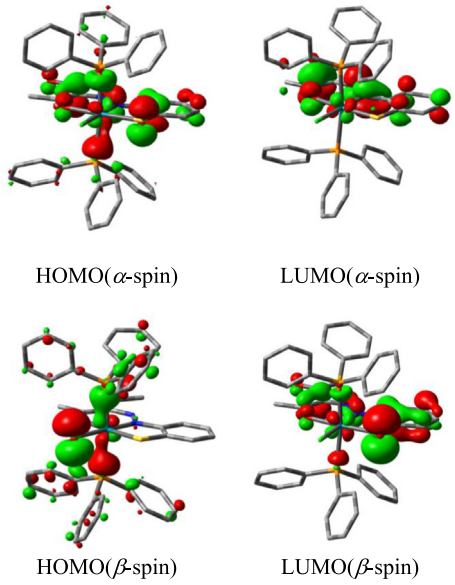

Fig. 5. Contour plots of selected molecular orbitals of $\mathbf{1}^+$. Isodensity value 0.04 e $Bohr^{-3}$.

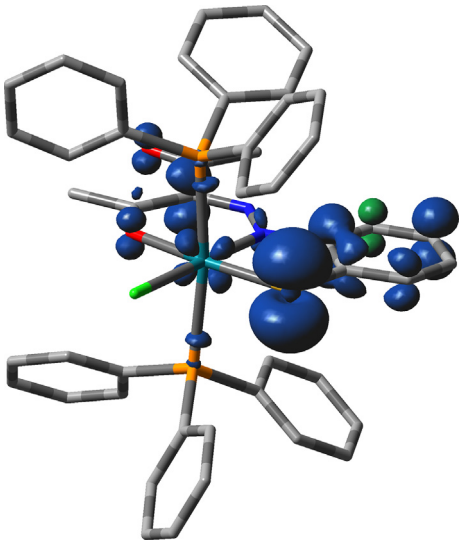

Fig. 6. Spin density plot of $\mathbf{1}^+$ (Rh, 2%; S, 57%). Isodensity value 0.004 e $Bohr^{-3}$.

complex **1**, different catalyst:substrate (C:S) ratios were tested. It was found that the conversions were excellent with C:S ratios of

Table 5
Effect of the C:S ratio, base and reaction time on the transfer hydrogenation of acetophenone.[a]

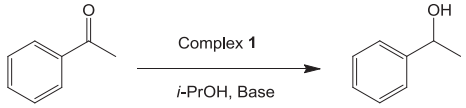

Entry	C:S ratio	Base	Time (h)	Conversion[b] (%)	TON[c]
1	1:300	KOH	3	71	213
2	1:300	KOH	4	82	246
3	1:300	KOH	5	98	294
4	1:300	KOH	7	98	294
5	1:300	KOH	10	98	294
6	1:300	NaOH	5	95	285
7	1:300	Na_2CO_3	5	49	147
8	1:300	CH_3COONa	5	39	117
9	1:300	KO^tBu	5	67	201
10	1:400	KOH	5	96	384
11	1:500	KOH	5	90	450
12	1:600	KOH	5	85	510
13	1:800	KOH	5	66	528
14	1:1000	KOH	5	43	430
15	1:1500	KOH	5	21	315

[a] Reaction conditions: acetophenone (3 mmol), complex **1** (10–2 μmol), catalyst: KOH 1:4 in *i*-PrOH (10 mL) at 80 °C.
[b] Conversion was determined by GC with undecane as an internal standard.
[c] Turnover number (TON) = mole of product/mol of catalyst.

1:300–1:400. With a decrease of the catalyst concentration, with C:S ratios of 1:500, 1:600, 1:800, 1:1000 or 1:1500, the transfer hydrogenation reactions proceed but a sharp decrease in the rates of conversion was observed for C:S ratios of 1:600–1:1500. The excellent conversion (96%) with a moderate turnover number (TON) was observed with the C:S ratio of 1:400. A series of ketones were screened for transfer hydrogenation reactions using a C:S ratio of 1:400 and KOH as the base in *i*-PrOH. The results are summarized in Table 6. The maximum conversion was observed for *p*-methoxyacetophenone (98%) to the corresponding alcohol. The conversions of other acetophenones were found to be in the range 89–97%. Excellent catalytic conversions were also achieved for cyclic ketones, such as cyclopentanone (95%), cyclohexanone (92%) and cycloheptanone (89%). Moreover, the catalytic efficiency of the present rhodium(III) complex towards transfer hydrogenation of ketones are comparable to reported rhodium catalysts [49–51].

4. Conclusion

Herein, a new rhodium(III) triphenylphosphine complex, [Rh$(PPh_3)_2$(L)Cl] (**1**) was synthesized by C—S cleavage of L-CH_2Ph. X-ray structure analysis confirms the distorted octahedral geometry around the rhodium ion. In a cyclic voltammetric study, the complex exhibits a thiophenolato-S to thiyl (S·) oxidation process

Table 6
Transfer hydrogenation of ketones using complex **1**.[a]

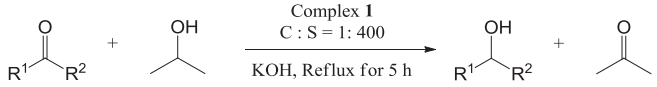

Entry	Ketones	Alcohols	Conversion (%)[b]	TON[c]	Entry	Ketones	Alcohols	Conversion (%)[b]	TON[c]
1	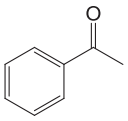	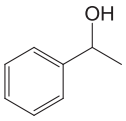	96.13 ± 0.51	385 ± 2	7	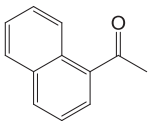	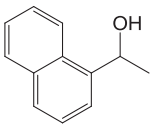	89.34 ± 0.25	357 ± 1
2	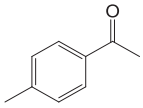	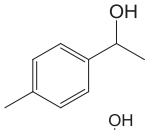	92.25 ± 0.50	369 ± 2	8	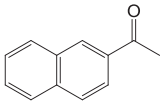	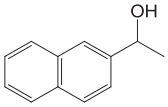	91.42 ± 0.25	366 ± 1
3	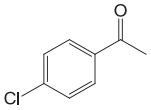	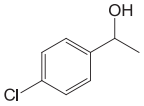	96.31 ± 0.24	385 ± 1	9	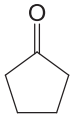	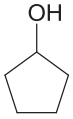	95.12 ± 0.27	380 ± 1
4	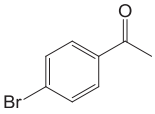	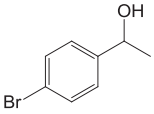	94.33 ± 0.36	377 ± 1	10	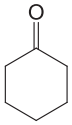	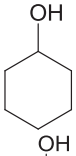	92.13 ± 0.22	369 ± 1
5	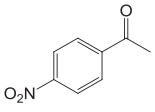	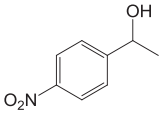	96.89 ± 0.50	388 ± 2	11	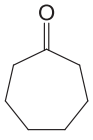	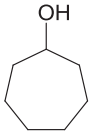	89.34 ± 0.51	357 ± 2
6	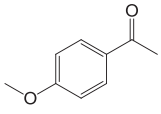	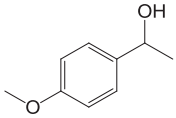	97.76 ± 0.40	391 ± 2	12	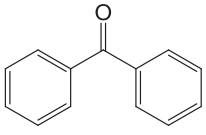	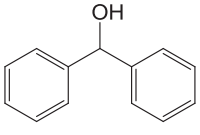	85.32 ± 0.50	341 ± 2

[a] Experimental conditions: reactions were carried out at 80 °C, ketone (3 mmol), Rh(III) complex (0.25 mol%), KOH (0.1 mmol), *i*-PrOH (10 mL).
[b] Conversions were determined by GC with undecane as an internal standard and were reported mean values with standard error of three runs.
[c] Turnover number (TON) = mole of product/mol of catalyst.

and azo(N=N) bond reduction. The redox properties are well interpreted by DFT studies. Vertical electronic transitions calculated by the TDDFT/CPCM method were used to interpret the UV–Vis spectrum of the complex and a good correlation between the experimental bands and the calculated transitions were observed. Moreover, the complex effectively catalyzed the transfer hydrogenation reaction of ketones with high yields in *i*-PrOH in the presence of a base.

Acknowledgements

Financial supports received from the Science and Engineering Research Board (SERB), New Delhi, India (YSS/2015/001533) is gratefully acknowledged. P. Roy and R. Naskar are thankful to UGC, New Delhi, India for fellowships.

Appendix A

CCDC 1495887 contains the supplementary crystallographic data the structure of **1**. These data can be obtained free of charge via http://www.ccdc.cam.ac.uk/conts/retrieving.html, or from the Cambridge Crystallographic Data Centre, 12 Union Road, Cambridge CB2 1EZ, UK; fax: (+44) 1223-336-033; or e-mail: deposit@ccdc.cam.ac.uk.

References

[1] L. Wang, W. Hea, Z. Yu, Chem. Soc. Rev. 42 (2013) 599.
[2] R. Tan, D. Song, Organometallics 30 (2011) 1637.
[3] S. Kundu, W.W. Brennessel, W.D. Jones, Organometallics 30 (2011) 5147.
[4] M.R. Grochowski, T. Li, W.W. Brennessel, W.D. Jones, J. Am. Chem. Soc. 132 (2010) 12412.
[5] M. Ma, J.R. Lohman, T. Liu, B. Shen, Proc. Natl. Acad. Sci. USA 112 (2015) 10359.
[6] S. Acharya, P. Bandyopadhyay, P. Das, S. Biswas, A.N. Biswas, J. Organomet. Chem. 866 (2018) 13.
[7] C.A. Tolman, J. Am. Chem. Soc. 92 (1970) 2956.
[8] C.A. Tolman, Chem. Rev. 77 (1977) 313.
[9] K. Ray, S.D. George, E.I. Solomon, K. Wieghardt, F. Neese, Chem. Eur. J. 13 (2007) 2783.
[10] M. Tamura, K. Tsuge, A. Igashira-Kamiyama, T. Konno, Inorg. Chem. 50 (2011) 4764.
[11] S.G. Modha, V.P. Mehta, E. Van der Eycken, Chem. Soc. Rev. 42 (2013) 5042.
[12] L. Wang, W. He, Z. Yu, Chem. Soc. Rev. 42 (2013) 599.
[13] J. Ito, H. Nishiyama, Tetrahedron Lett. 55 (2014) 3133.
[14] R. Malacea, R. Poli, E. Manoury, Coord. Chem. Rev. 254 (2010) 729.
[15] R. Patchett, I. Magpantay, L. Saudan, C. Schotes, A. Mezzetti, F. Santoro, Angew. Chem., Int. Ed. 52 (2013) 10352.
[16] W.J. Ye, M. Zhao, Z.K. Yu, Chem. Eur. J. 18 (2012) 10843.
[17] S. Biswas, D. Sarkar, P. Roy, T.K. Mondal, Polyhedron 131 (2017) 1.
[18] S. Biswas, D. Sarkar, S. Kundu, P. Roy, T.K. Mondal, J. Mol. Struct. 1099 (2015) 297.
[19] S. Biswas, P. Roy, S. Jana, T.K. Mondal, J. Organomet. Chem. 846 (2017) 201.
[20] A.K. Pramanik, D. Sarkar, T.K. Mondal, J. Mol. Struct. 1099 (2015) 92.
[21] G.M. Sheldrick, Acta Cryst. A64 (2008) 112–122.
[22] A.D. Becke, J. Chem. Phys. 98 (1993) 5648.
[23] C. Lee, W. Yang, R.G. Parr, Phys. Rev. B 37 (1988) 785.
[24] P.J. Hay, W.R. Wadt, J. Chem. Phys. 82 (1985) 270.
[25] W.R. Wadt, P.J. Hay, J. Chem. Phys. 82 (1985) 284.
[26] P.J. Hay, W.R. Wadt, J. Chem. Phys. 82 (1985) 299.
[27] R. Bauernschmitt, R. Ahlrichs, Chem. Phys. Lett. 256 (1996) 454.
[28] R.E. Stratmann, G.E. Scuseria, M.J. Frisch, J. Chem. Phys. 109 (1998) 8218.
[29] M.E. Casida, C. Jamorski, K.C. Casida, D.R. Salahub, J. Chem. Phys. 108 (1998) 4439.
[30] V. Barone, M. Cossi, J. Phys. Chem. A 102 (1998) 1995.
[31] M. Cossi, V. Barone, J. Chem. Phys. 115 (2001) 4708.
[32] M. Cossi, N. Rega, G. Scalmani, V. Barone, J. Comput. Chem. 24 (2003) 669.
[33] Gaussian 09, Revision D.01, M.J. Frisch, G.W. Trucks, H.B. Schlegel, G.E. Scuseria, M.A. Robb, J.R. Cheeseman, G. Scalmani, V. Barone, B. Mennucci, G.A. Petersson, H. Nakatsuji, M. Caricato, X. Li, H.P. Hratchian, A.F. Izmaylov, J. Bloino, G. Zheng, J.L. Sonnenberg, M. Hada, M. Ehara, K. Toyota, R. Fukuda, J. Hasegawa, M. Ishida, T. Nakajima, Y. Honda, O. Kitao, H. Nakai, T. Vreven, J.A. Montgomery, Jr., J.E. Peralta, F. Ogliaro, M. Bearpark, J.J. Heyd, E. Brothers, K.N. Kudin, V.N. Staroverov, R. Kobayashi, J. Normand, K. Raghavachari, A. Rendell, J. C. Burant, S.S. Iyengar, J. Tomasi, M. Cossi, N. Rega, J.M. Millam, M. Klene, J.E. Knox, J.B. Cross, V. Bakken, C. Adamo, J. Jaramillo, R. Gomperts, R.E. Stratmann, O. Yazyev, A.J. Austin, R. Cammi, C. Pomelli, J.W. Ochterski, R.L. Martin, K. Morokuma, V.G. Zakrzewski, G.A. Voth, P. Salvador, J.J. Dannenberg, S. Dapprich, A.D. Daniels, Ö. Farkas, J.B. Foresman, J.V. Ortiz, J. Cioslowski, D.J. Fox, Gaussian, Inc., Wallingford CT (2009).
[34] N.M. O'Boyle, A.L. Tenderholt, K.M. Langner, J. Comput. Chem. 29 (2008) 839.
[35] S. Roy, S. Pramanik, T. Ghorui, S. Dinda, S.S. Patra, K. Pramanik, New J. Chem. 42 (2018) 5548.
[36] M. Fátima, C.G. da Silva, A.M. Trzeciak, J.J. Ziólkowski, A.J.L. Pombeiro, J. Organomet. Chem. 620 (2001) 174.
[37] U. Das, T. Ghorui, B. Adhikari, S. Roy, S. Pramanik, K. Pramanik, Dalton Trans. 44 (2015) 8625.
[38] S. Biswas, P. Roy, T.K. Mondal, J. Mol. Struct. 1142 (2017) 110.
[39] K. Pramanik, U. Das, B. Adhikari, D. Chopra, H. Stoeckli-Evans, Inorg. Chem. 47 (2008) 429.
[40] A.H. Obaid, N.G. Stracey, C.D. Incarvito, B.Q. Mercado, J. Parr, J. Organomet. Chem. 830 (2017) 74.
[41] S.A. Talouki, G. Grivani, P. Crochet, V. Cadierno, Inorg. Chim. Acta 456 (2017) 142.
[42] T.S. Manikandan, S. Saranya, R. Ramesh, Tetrahedron Lett. 57 (2016) 3764.
[43] L.O. Nindakova, N.M. Badyrova, V.V. Smirnov, S.S. Kolesnikov, J. Mol. Catal. A 420 (2016) 149.
[44] N. Mukherjee, R. Gawin, S.J. Czarnocki, R. Gajda, M. Malinska, K. Wozniak, A. Kajetanowicz, K. Grela, J. Organomet. Chem. 867 (2018) 359.
[45] V.R. Landaeta, A.D. Salazar-La Rosa, R.E. Rodriguez-Lugo, Inorg. Chim. Acta 470 (2018) 303.
[46] M. Sun, J. Campbell, G. Kang, H. Wang, B. Ni, J. Organomet. Chem. 810 (2016) 12.
[47] J.M. Gichumbi, B. Omondi, H.B. Friedrich, Eur. J. Inorg. Chem. (2017) 915.
[48] J. Holmes, C.M. Pask, C.E. Charlotte, Dalton Trans. 45 (2016) 15818.
[49] M.U. Raja, R. Ramesh, K.H. Ahn, Tetrahedron Lett. 50 (2009) 7014.
[50] K. Rafikova, N. Kystaubayeva, M. Aydemir, C. Kayan, Y.S. Ocak, H. Temel, A. Zazybin, N. Gürbüz, İ. Özdemir, J. Organomet. Chem. 758 (2014) 1.
[51] M. Aydemir, N. Meric, C. Kayan, F. Ok, A. Baysal, Inorg. Chim. Acta 398 (2013) 1.